# FAULT STRUCTURE OF THE PUNTA MONTALVA USING HIGH-RESOLUTION DEMS

By

LAUREN J. WEILERT

Bachelor of Science in Geology

Oklahoma State University

Stillwater, Oklahoma

2020

Submitted to the Faculty of the
Graduate College of the
Oklahoma State University
in partial fulfillment of
the requirements for
the Degree of
MASTER OF SCIENCE
July, 2022

FAULT STRUCTURE OF THE PUNTA MONTALVA

FAULT USING HIGH-RESOLUTION DEMS

Thesis Approved:

Dr. Daniel A. Laó Dávila

Thesis Adviser

Dr. Ahmed Ismail

Dr. Mohamed Abdel Salam

ACKNOWLEDGEMENTS

I would like to acknowledge and give my biggest thanks to my advisor Dr. Daniel A. Laó-Dávila for making this work possible. His patience and guidance carried me throughout my graduate career. I would also like to thank Dr. Chelsea Scott for her knowledge and guidance over vertical differencing. A big thanks goes my lab colleagues Melina Lazar and Oyewande Ojo for their constant support and laughter they have provided me these past two years. They have truly made this an enjoyable experience. Finally, I would like to give a special thanks my mother and my brother for constantly pushing me to work hard and to not give up. Without them I would have not made it this far.

Name: LAUREN J. WEILERT

Date of Degree: JULY, 2022

Title of Study: FAULT STRUCTURE OF THE PUNTA MONTALVA FAULT USING HIGH-RESOLUTION DEMS

Major Field: GEOLOGY

Abstract: The Punta Montalva Fault is an active left-lateral strike-slip fault that slipped during the 2019-2020 Puerto Rico seismic sequence. Not much is known about the structure, segmentation, and spatial extent of the fault as it is obscured under thick vegetation and is difficult to access. This study used high-resolution topographic data to map the Punta Montalva Fault's structure, segmentation, and spatial extent and conduct vertical differencing of topography to determine if slip is detectable along the fault from 2004 to 2018. A 0.5 m resolution bare-earth digital elevation model (DEM) derived from a 2018 airborne light detection and ranging (LiDAR) survey and a 1 m resolution 2018 DEM was used to map the Punta Montalva Fault from Punta Montalva to Ensenada Las Pardas. High-resolution mapping revealed that the Punta Montalva Fault is comprised of three main fault segments on the surface and two fault scarps in they bathymetry. The fault segments on the surface and bathymetry illustrate both strike-slip and normal fault movement. The DEM revealed scarps, dragged and cut layers, and a duplex structure. The total length of the fault segments exposed on the surface is approximately 2.67 km long. However, if the Punta Montalva Fault is continuous beneath the surface, its total fault length would be approximately 7.97 km long. These factors are beneficial to determine the Punta Montalva Fault's surface rupture length.

Two LiDAR datasets from 2004 and 2018 were used to conduct vertical differencing of topography along the Punta Montalva Fault from Punta Montalva to Ensenada Las Pardas. Both the 2004 and 2018 LiDAR datasets were processed into digital terrain models (DTMs) and then subtracted from one another to visualize the vertical change in topography that has occurred in the 14 years along the Punta Montalva Fault. Vertical differencing results along the Punta Montalva Fault were unconclusive due to poor quality of the 2004 DEM.

TABLE OF CONTENTS

LIST OF FIGURES

Figure Page

# CHAPTER I

## INTRODUCTION

The island of Puerto Rico has been affected by damaging earthquakes. With a population of around 3.3 million (US Census, 2021), Puerto Rico is vulnerable to earthquake hazards, thus making it necessary to research the danger they pose to its inhabitants. Puerto Rico lies on the eastern end of the Greater Antilles and is part of the Puerto Rico-Virgin Islands Microplate (Jansma et al., 2000). The microplate is in the complex ~250-km-wide deformation zone of the North American-Caribbean plate boundary (Fig. 1; Jansma et al., 2000). The North American plate moves westward 2 cm/year relative to the Caribbean plate as determined by GPS geodesy (Jansma et al., 2000; Calais et al., 2002). The oblique subduction zone subjects Puerto Rico to major tectonic strike-slip, reverse, and normal faulting around the island and accommodates overall plate movement (McCann & Pannington, 1990). Puerto Rico is bound by the Puerto Rico Trench to the north, the Muertos Trough to the south, the Mona Passage to the west, and the Anegada Passage to the east (Masson and Scanlon, 1991; Jansma et al., 2005; Huérfano et al., 2005; Benford et al., 2012). Active offshore faulting is a significant contributor to the seismicity in Puerto Rico. However, there are active faults on land, particularly in the southwestern region of the island.

The Lajas Valley, located in the southwestern corner of Puerto Rico, contains the most onshore shallow seismic activity throughout the whole island (Fig. 2; Mann et al., 2005). The large seismic sequence that began on December 28, 2019 in the southeast region of the Lajas Valley produced over 14 earthquakes M 4.5 or larger, with thousands of smaller subsequent earthquakes (Fig. 2; López et al., 2020). The largest magnitude earthquakes recorded during this seismic sequence was a M 5.8 on January 6, a M 6.4 on January 7, and M 5.9 on January 11 (López et al., 2020). The location of this seismic sequence suggests the presence of a previously

unknown normal fault offshore and the activation of a southeasterly seaward extension of the Punta Montalva Fault (López et al., 2020).

The Punta Montalva fault is an active left-lateral strike-slip fault located in the southeastern region of the Lajas Valley (Addarich-Martínez, 2009; Roig-Silva et al., 2009). Analysis of the event distribution and focal mechanisms of the 2019-2020 southwestern Puerto Rico seismic sequence indicated that the moment magnitude (Mw) 6.4 earthquake that occurred on January 7, 2020 resulted from a normal fault with the foreshocks and aftershocks occurring along the Punta Montalva Fault (López et al., 2020; ten Brink et al., 2022). It was later discovered that the Punta Montalva Fault had little responsibility in the initiation 2019-2020 seismic sequence that occurred several kilometers ENE of the southeastern end of the fault (ten Brink et al., 2022). However, moderate-sized strike-slip earthquakes were produced along 5 km of the Punta Montalva Fault's southeastern end in June 2020, five months after the Mw 6.5 on January 7, 2020 (ten Brink et al., 2022).

The structure and spatial extent of the Punta Montalva Fault is not well understood because of its remote location and difficulty to access under vegetation. Whether strain is localized into a single fault, in segments, or distributed in a wide deformation zone is still unknown. Furthermore, slip rates in southwestern Puerto Rico are poorly understood. A well-constrained fault length, structure, and strain accommodation model is important to address the seismic hazard of the fault.

In this study we (1) mapped the Punta Montalva Fault through high-resolution data to provide an improved characterization of the structure of the fault, and (2) conducted vertical differencing on two Light Detection and Ranging (LiDAR) datasets from 2004 and 2018 derived from airborne surveys to determine if slip was detectable along the fault during this time frame. Analysis of the vertical differencing between the two LiDAR datasets would reveal the surface changes the Punta Montalva Fault has undergone in 14 years if enough slip was accommodated. We hypothesize that (1) an improved delineation of the structures of the Punta Montalva Fault can be obtained from a high-resolution bare-earth 2018 DEM derived from LiDAR data, and (2) that slip on the Punta Montalva Fault between 2004 and 2018 can be detected through vertical differencing between the airborne LiDAR surveys. The high-resolution bare-earth 2018 DEM will provide further insight into the characterization of the Punta Montalva Fault that has not been obtained prior due to it being hidden under thick vegetation. We will also test if the 14-year time span between the 2004 and 2018 datasets can detect vertical displacement along the Punta

Montalva Fault. This information would be beneficial to further comprehend the seismic potential of the Punta Montalva Fault by constraining its length and a slip measurement that could better indicate how strain has been accommodated in the area.

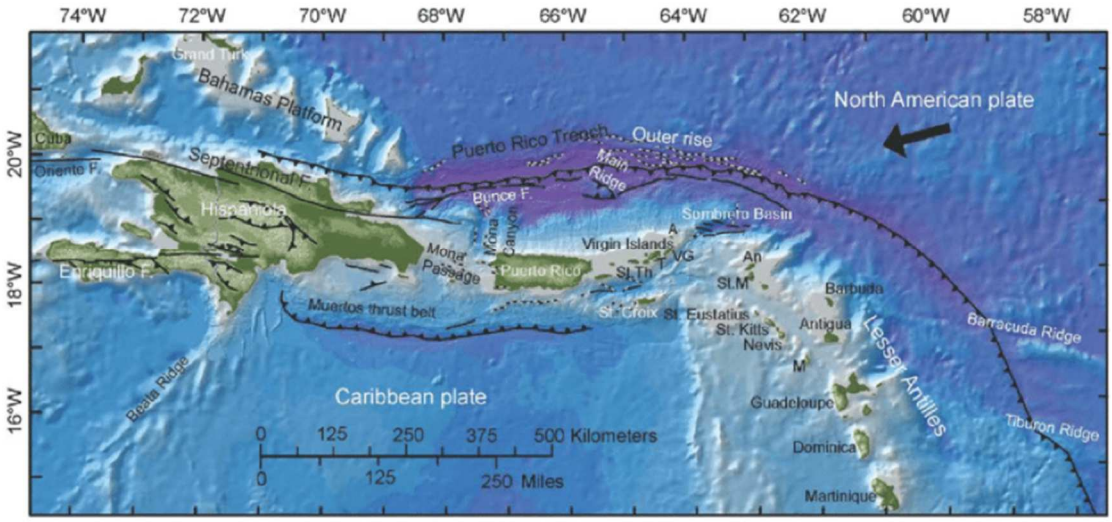


**Figure 1**: Regional tectonic map of Hispaniola, Puerto Rico, Virgin Islands, and the Northern Lesser Antilles in the northern Caribbean (Flores et al., 2012). St. Th = Thomas; T = Tortola; VG = Virgin Gorda; A = Anegada; An = Anguilla; St. M = St. Martin/St. Maarteen; M = Montserrat. Line with teeth represents thrust faulting. Dashed lines represent normal or mixed normal and strike-slip faults. Solid lines represent strike-slip faults. Arrows represent the direction of plate motion of the North American plate relative to the Caribbean plate.

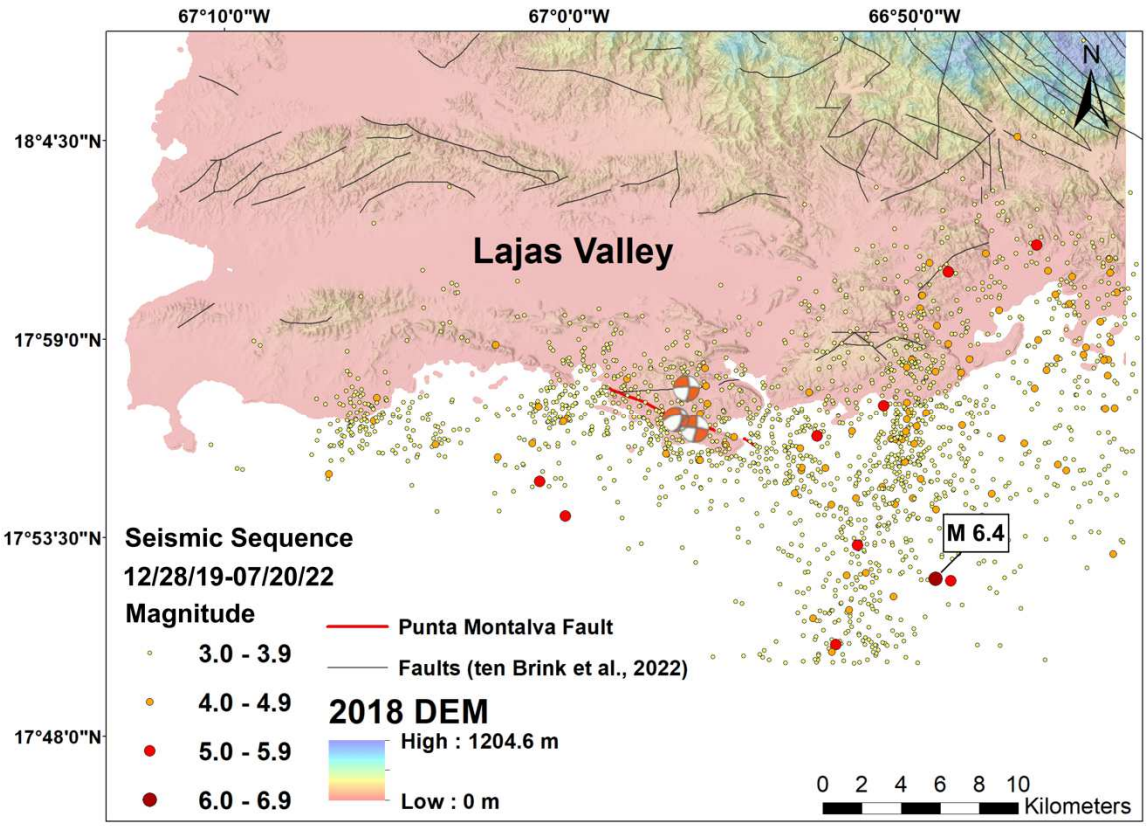


**Figure 2**: Shaded relief map of the Lajas Valley in southwestern Puerto Rico showing the seismic events processed by the Puerto Rico Seismic Network between December 28, 2019 and July 20, 2022. Colored circles show 1,868 seismic events that occurred during this time (magnitude greater than or equal to 3.0). Beachballs are the focal mechanisms of the three earthquakes that occurred along the Punta Montalva Fault five months after the M 6.4 earthquake in June (ten Brink et al., 2022).

# CHAPTER II

## REVIEW OF LITERATURE

### *2.1 Faulting in Southwestern Puerto Rico*

The southwestern region of Puerto Rico is characterized by "basin and range"-like topography (Joyce et al., 1987). Analysis of offshore seismic-reflection studies suggests the formation of east-west trending half grabens and N-S extension (Dolan et al., 1998; Chaytor & Uri, 2010). The Lajas Valley is in the southernmost part of this "basin and range" topography and is the site that contains the greatest concentration of onshore shallow seismic activity throughout all of Puerto Rico (Mann et al., 2005). The Lajas valley is an east-west striking depression that is 30-km-long and 1.5 to 9.0 km wide that is characterized by gently inclined hills to the north and steeply sloping hills with alluvial fans to the south. Through observation of geomorphology, it is suggested that Quaternary faulting controls the shape of the Lajas Valley (Joyce et al., 1987). Trenching across a previously known fault scarp belonging to the South Lajas Fault on the southern edge of the Lajas Valley uncovered a fault zone disrupting alluvial deposits (Fig. 3; Prentice & Mann, 2005). Radiocarbon dating of the Quaternary alluvial fan deposits revealed that the South Lajas Fault is an active Holocene fault that has shown movement in the past ~5,000 years (Prentice & Mann, 2005). The South Lajas Fault trends E-W and it is suggested to be ~50 km long (Fig. 3; Prentice & Mann, 2005). Re-interpreted total intensity magnetic and seismic reflection data along the western shore of Boquerón in the Lajas Valley revealed a previously unmapped fault offshore, the Northern Boquerón Bay Fault (Ocasio, 2004).

The Northern Boquerón Bay Fault is a W-NW deeply seated structure within the crust and is suggested to extend into the Lajas Valley (Fig. 3; Ocasio, 2004). Additional investigations through multichannel and high-resolution seismic-reflection data concluded that the Norther Boquerón Bay Fault coincides with a boundary in the Boquerón Mangrove Forest that is interpreted to be a normal fault (Roig-Silva & Asencio, 2007; Kaye, 1957).

*2.2 The Punta Montalva Fault*

The Punta Montalva Fault is a NW-SE striking fault located to the SE of the Lajas Valley (Fig. 3). The fault was recognized by geological mapping, remote sensing, displaced and truncated streams, and geomorphological features (Roig-Silva, 2003; Addarich-Martínez, 2009; Roig-Silva et al., 2009; Rivera-Santiago, 2009; Adames-Corraliza, 2017). The fault cuts Miocene Ponce Limestone, which contains steeply inclined strata near the fault (Addarich-Martínez, 2009). Geomorphological features that suggest left-lateral displacement include the parallel alignment of intermittent streams to the lineament of the fault, a left-lateral displaced stream in the order of ~200 m, and a left-lateral displaced stream valley also in the order of ~200 m (Rivera-Santiago, 2009). Truncated drainages were also found that flow perpendicular across the Punta Montalva Fault that display steps or changes in gradient (Adames-Corraliza, 2017). It was concluded that the surface rupture length of the Punta Montalva Fault from Punta Montalva to Ensenada Las Pardas was at least 6 km long and at a shutter ridge alluvial valley around 35 m wide (Adames-Corraliza, 2017). Interpretation of GPR results revealed three near-surface fault ruptures that occurred in the late Quaternary suggesting that the Punta Montalva Fault is active (Adames-Corraliza, 2017).

Roig-Silva et al. (2013) suggest that the Punta Montalva Fault is part of a major through-going left-lateral strike-slip fault zone called the North Boquerón Bay-Punta Montalva Fault zone (NBPMFZ) that cuts across the Lajas Valley (Fig. 3). Strain partitioning was suggested along the NBPMFZ and first-motion focal mechanism solutions suggested left-lateral strike-slip with a component of compression (Roig-Silva et al., 2013). However, there is not enough evidence to support that the Punta Montalva and the North Boquerón faults are connected at depth.

Analysis of the focal mechanisms and event distribution of one of the largest earthquakes recorded in the seismic sequence that began on December 28, 2019 in southwestern Puerto Rico was discovered to be produced by a normal fault offshore (ten Brink et al., 2022). The Mw 6.4 earthquake ruptured offshore southeast of the Punta Montalva Fault at a depth of 8.5 km, then continued to propagate downwards to 15 km after the initial rupture (ten Brink et al., 2022). It was discovered that the Punta Montalva Fault had no relation to the activation of this seismic swarm, but did experience strike-slip earthquakes onshore along the fault five months after the Mw 6.4 earthquake in June 2020 (ten Brink et al., 2022).

Study of the 2019-2020 Puerto Rico seismic sequence conducted through kinematic source inversion of the five largest earthquakes determined the depth distribution of seismicity

during this sequence along the Punta Montalva Fault extended for 30 km in a WNW-ESE direction and had a depth shallower than 10 km (Vičič et al., 2021). It was determined that the Punta Montalva Fault and a fault to the north form a system of parallel strike-slip faults with a normal fault forming an oblique structure between them (Vičič et al., 2021). Additionally, it was concluded that an orthogonal fault connects the two strike-slip parallel faults, bounded by the northern strike-slip fault to the north and continues past the Punta Montalva Fault in the south (Vičič et al., 2021). It was suggested that this seismic sequence was the result of strain partitioning due to the oblique subduction of the Caribbean plate underneath Puerto Rico (Vičič et al., 2021). It was also suggested that the fluids that are being released from the subducting oceanic crust are draining through permeable fluid conduits, like the Punta Montalva Fault (Vičič et al., 2021).

Synthetic aperture radar interferometry (InSAR) images and measurements from the Copernicus Sentinel-1A and -1B satellites from the European Space Agency and the Advanced Land Observation Satellite-2 (ALOS-2) from the Japanese Aerospace Exploration Agency were used to analyze the deformation of the seismic sequence (ten Brink et al., 2022). The combination of the InSAR and ALOS-2 data from September 2019 to January 20, 2020 revealed part of the Punta Montalva Fault experienced 8 cm of slip at the surface (ten Brink et al., 2022). It is inferred that the slip occurred as a result of either the large foreshocks or aftershocks of the Mw 6.4 earthquake that occurred on January 7, 2020 (ten Brink et al., 2022).

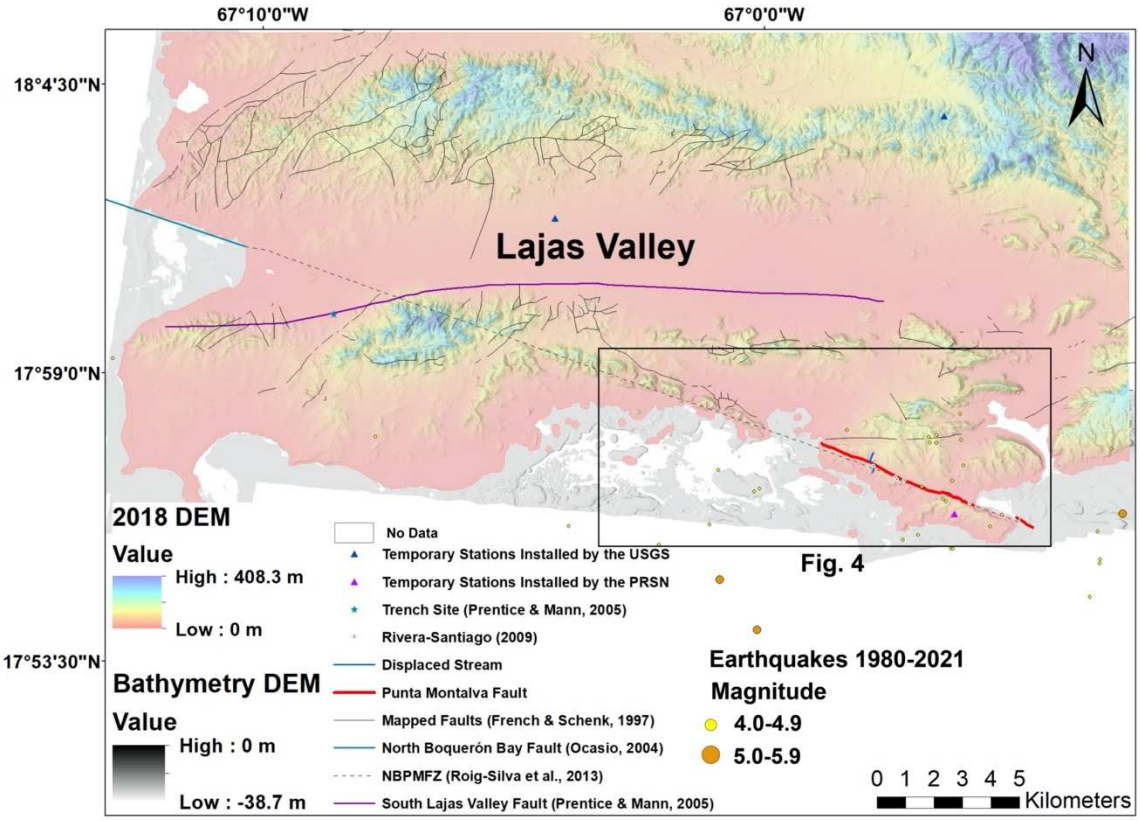


**Figure 3**: Shaded relief map of the topography and bathymetry of southwestern Puerto Rico showing faults and earthquakes using a multidirectional hillshade. The earthquakes, using the Richter magnitude scale, are from January 1, 1980 to January 1, 2021.

### *2.3 Geology of the Study Area*

The geology of the study area is shown in Figure 4 The Miocene Ponce Limestone Formation ranges in thickness from 50 m to 200 m and rests on the Oligocene Juana Díaz Formation and Cretaceous sedimentary and volcanic rocks (Fig. 4; Monroe, 1980; Addarich, 2009). The Ponce Limestone covers the majority of the topography in the study area from Punta Montalva to Ensenada Las Pardas. The Ponce Limestone covers an area of 7 $km^2$ extending north into the Sabana Grande quadrangle (Llerandi-Roman, 2004), east into the Yauco quadrangle (Krushensky et al., 1979), and west into the Cabo Rojo and Parguera quadrangles (Volckmann, 1984). In the study area, the Ponce Limestone Formation consists of white, light orange, and pale brown massive to laminated bedded bioclastic grainstone, wackestone, and packstone (Addarich-Martínez, 2009). The hills formed by the Ponce Limestone formation have medium slopes, except

where it comes in contact with the Juana Díaz Formation where the slopes are steeper because of their greater resistance to weathering (Addarich-Martínez, 2009). Post-Ponce Limestone deformation consists of sub-horizontal to shallowly inclined strata that suggest the formation has been subjected to little tectonic deformation (Addarich-Martínez, 2009). Addarich-Martínez, (2009) suggests that karst topography is not common in the Ponce Limestone formation, though few caves were observed.

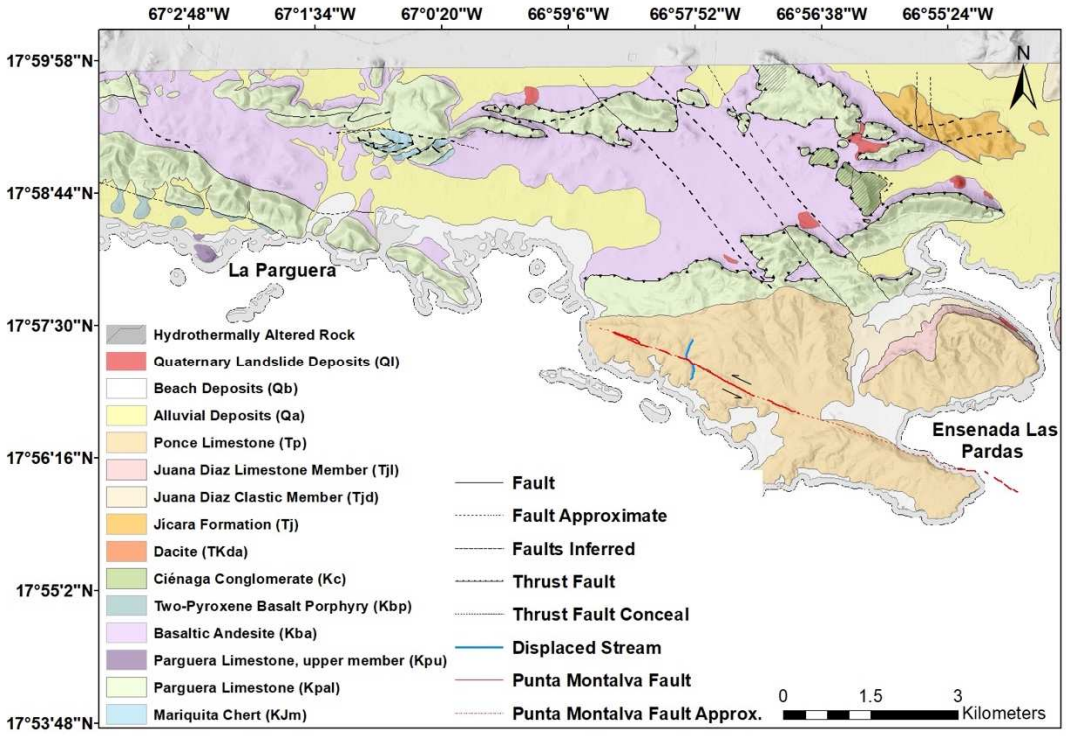


**Figure 4:** Geologic map derived from Volckmann (1984) and Addarich-Martínez (2009) of the high-resolution mapping study area using a multidirectional hillshade. The red line is the Punta Montalva Fault's trend from this study. Arrows indicate left-lateral strike-slip movement.

# CHAPTER III

# METHODOLOGY

## *3.1 Data*

I used two different datasets from 2004 and 2018 to map and determine movement along the Punta Montalva Fault by conducting vertical differencing using airborne LiDAR surveys. The LiDAR datasets from 2004 and 2018 were acquired from the National Oceanic and Atmospheric Administration (NOAA) data access viewer website. The 2004 airborne LiDAR survey was collected by the U.S. Army Corps of Engineers, Jacksonville District and has a horizontal accuracy of 1 m, vertical accuracy of 18.6 cm, estimated spacing of 1 m, and contains ground point classification from classes 1 (unclassified) and 2 (ground; Fig. 5a). The 2018 airborne LiDAR survey was collected by the U.S. Geological Survey and has a horizontal accuracy of 34.1 cm, vertical accuracy of 6.8 cm, estimated point spacing of 0.35 m, and contains ground point classification from classes 1 (unclassified), 2 (ground), 7 (low noise), 8 (model key/reserved), 9 (water), 17 (bridge decks), 18 (high noise), and 20 (ignored ground due to breakline proximity; Fig. 5b).

I used two high-resolution DEMs, a bathymetry DEM and a DEM processed from the 2018 LiDAR dataset, to map the Punta Montalva Fault on the surface and at shallow bathymetry. The bathymetry DEM was derived from an airborne LiDAR survey collected in 2018 by the U.S. Army Corps of Engineers that has a horizontal accuracy of 1 m, vertical accuracy of 10 cm, and a cell size one 1 m. The 2018 DEM was created only using ground point classification from class 2 (ground) by the U.S. Geological Survey and has a cell size of 0.5 m, vertical accuracy of 6.83 cm, and horizontal accuracy of 34.1 cm.

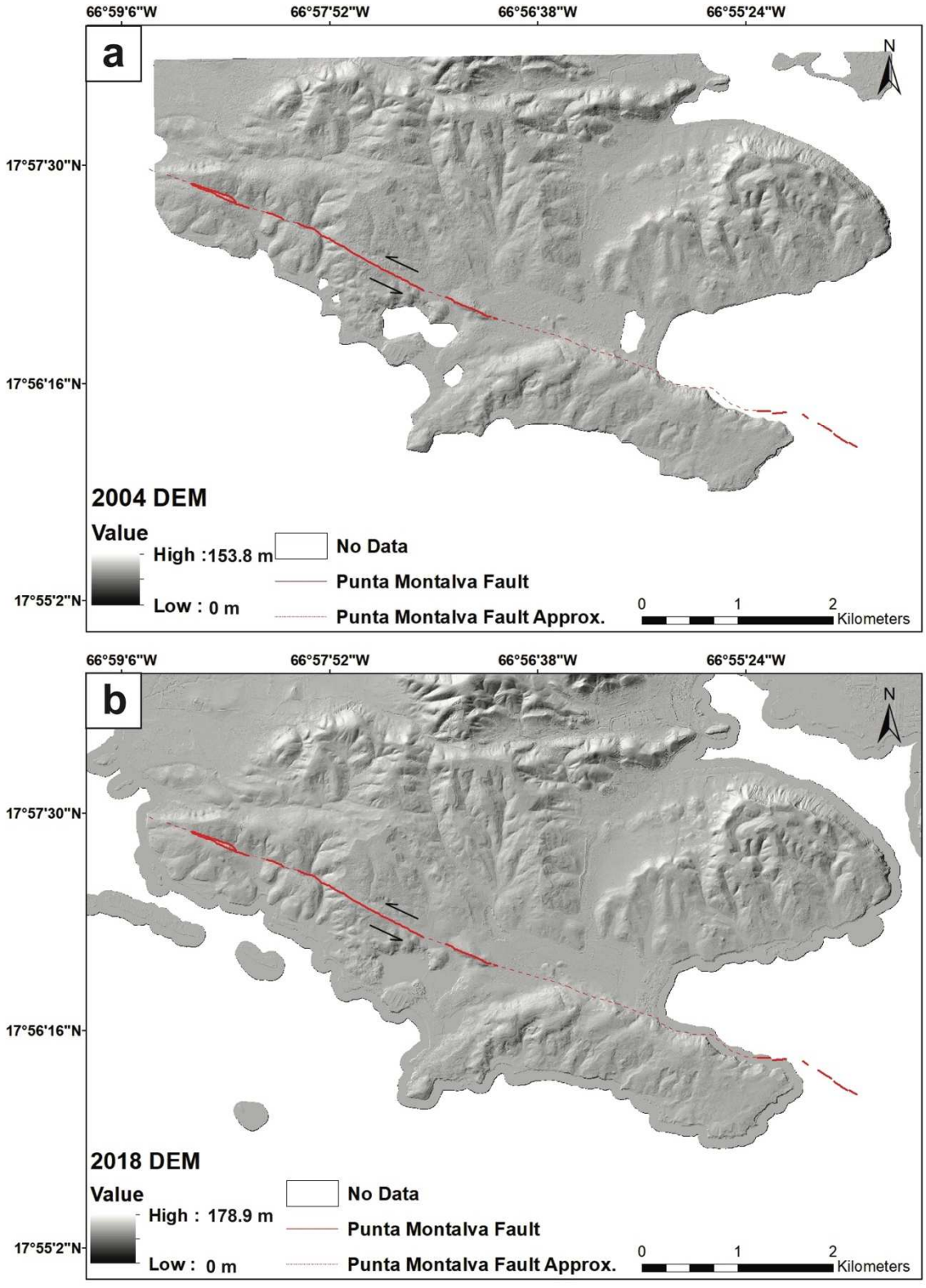


**Figure 5**: (a) Shaded relief map created from the 2004 LiDAR dataset containing class 2 (ground) point classification using a hillshade angle of 315°. The red line is the approximate trend of the Punta Montalva

Fault from this study. Arrows indicate left-lateral strike-slip movement. (b) Shaded relief map created from the 2018 LiDAR dataset containing class 2 (ground) point classification using a hillshade angle of 315°.

### *3.2 High-Resolution Mapping*

I used two separate DEMs to map the Punta Montalva Fault on the surface and at shallow bathymetry. I used the high-resolution (0.50 m) DEM derived from the 2018 LiDAR dataset processed by the U.S. Geological Survey to map the Punta Montalva Fault on the surface, and the high-resolution (1 m) bathymetry DEM processed by the U.S. Army Corps of Engineers to map the Punta Montalva Fault at shallow bathymetry. Using ArcGIS, two hillshades with Azimuth angles of 45° and 315° were processed and applied to the 2018 DEM and 2018 bathymetry DEM, as well as a multidirectional hillshade to provide more depth and detail to the topography and bathymetry. The extent of the area I used to map the Punta Montalva Fault ranges from La Parguera in the northwest to Ensenada Las Pardas in the southeast. Fault scarps in the surrounding area were also observed and mapped to further our understanding of how they interact with the Punta Montalva Fault. This was conducted by the construction of cross-cutting sections (perpendicular to the fault strikes) in the surrounding area to better visualize the fault scarps. Strike and dip measurements were acquired by obtaining the elevation and coordinates from the 2018 DEM and inputting them into an excel file that calculates three-point problems (Martinez-Torres et al., 2012).

### *3.3 Vertical Differencing*

Vertical differencing is the subtraction of raster-based DEMs that can be performed on grids generated from point cloud data or original raster topography (Scott et al., 2021). This technique is able to capture geological processes such as river erosion, earthquakes (Oskin et al., 2012; Clark et al., 2017), landslides (Lucieer et al., 2014), volcanic eruptions (Albino et al., 2015), and flooding (Izumida et al., 2017). By applying vertical differencing on the two LiDAR datasets, I was able to visualize any vertical change in the topography along the Punta Montalva Fault that has occurred in the 14-year time span.

Bare-earth models, or Digital Terrain Models (DTMs), were processed to compare the 2004 and 2018 LiDAR datasets through vertical differencing. Only ground point classification from class 2 (ground) was used to construct the DTMs for both the 2004 and 2018 LiDAR datasets. Before I made the DTMs, I manipulated the LiDAR point cloud data to provide better results and to also prepare the data to go through vertical differencing. Since vertical differencing is a subtraction of rasters from a cell-by-cell basis, both datasets needed to be manipulated into

one common model. I first used lasgrid from the LAStools software to make both the LiDAR point cloud datasets have a grid size of 1. I then input the newly gridded LiDAR point cloud datasets into las2dem from the LAStools software. In las2dem, I made sure both datasets had the same coordinate system and projection, then finally exported the DTMs created from the 2004 and 2018 LiDAR point clouds. Once I had both DTMs, I then begin subtracting them using the raster calculator tool in QGIS to show the difference in elevation between the two rasters. To accurately subtract one raster from another, the "compare" or "pre" dataset needs to be subtracted from the "reference" or "post" dataset (Scott et al., 2021). Therefore, I subtracted the 2004 DTM (compare) from the 2018 DTM (reference). The final product was a DEM topographic hillshade that depicts the upward or downward changes in topography that occurred in the 14-year time span.

# CHAPTER IV

# RESULTS AND DISCUSSION

## *4.1 Results*

### *4.1.1 High-Resolution Mapping*

Examination of the high-resolution 2018 DEM and bathymetry DEM revealed that the Punta Montalva Fault is not a single fault but comprised of multiple fault segments that are moderately distributed on the surface and at shallow bathymetry (Fig. 6). The Punta Montalva Fault displays a strong lineament on the surface that trends approximately 110° to 115° from Punta Montalva to Ensenada Las Pardas. Onshore, the Punta Montalva Fault has prominent surface exposure in three main segments, respectively named fault segments 1, 2, and 3. Offshore, additional fault scarps were discovered in the bathymetry that displays both strike-slip and normal fault movement. The total length of the exposed fault segments on the surface is approximately 2.67 km long. However, if the Punta Montalva Fault is continuous underneath the surface, the total fault length would be approximately 7.97 km from Punta Montalva to the bathymetry fault segments off the coast of the peninsula at Ensenada Las Pardas.

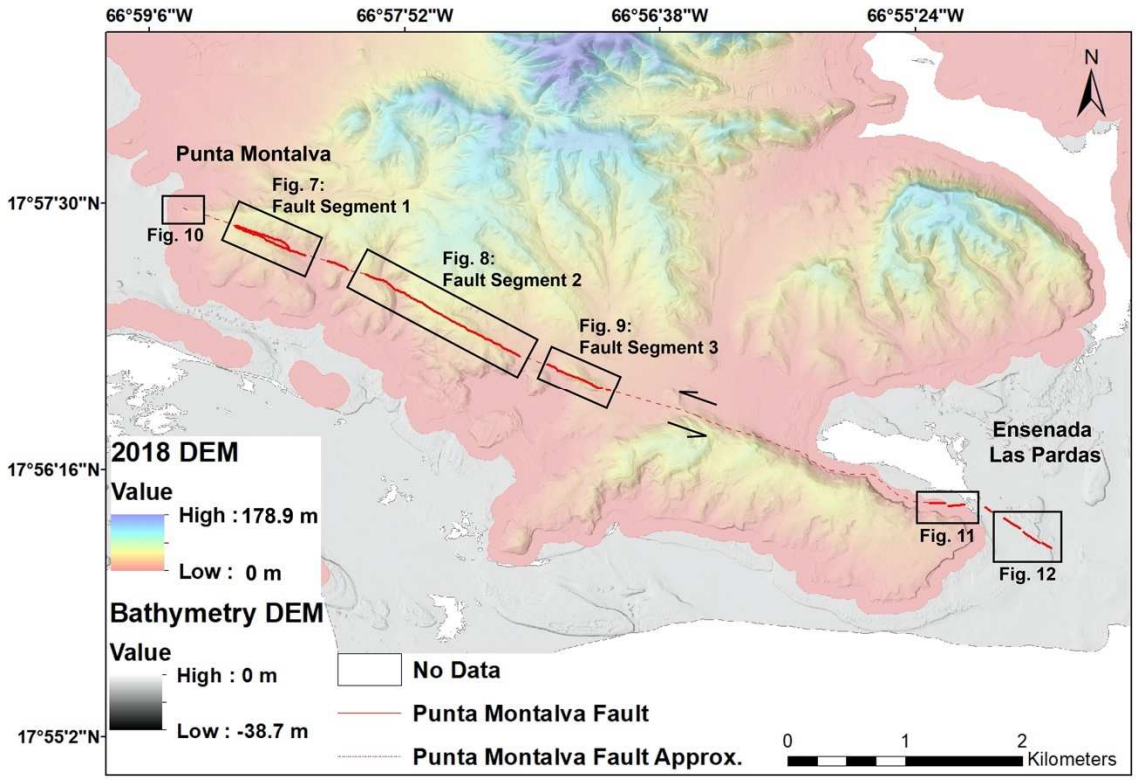


**Figure 6**: Shaded relief map of the topography and bathymetry using a multidirectional hillshade. The red line is the Punta Montalva Fault's trend from this study. The red dashed line is the approximate trend of the Punta Montalva Fault from this study. Arrows indicate left-lateral strike-slip movement. Black rectangles indicate the locations of the fault segments exposed on the surface and at shallow bathymetry highlighted in figures 7-12.

Fault segment 1 is approximately 655 m long and the fault scarp is around 6 m wide (Fig. 7). There appears to be a separate fault segment to the north approximately 512 m long that connects with the northwestern and southwestern ends of the main fault segment. The orientation of bedding is similar on the north and south sides of the fault segments. Bedding orientation north of the fault segments is 166°, 7°SW, while bedding orientation south of the fault segments is 176°, 4°SW. Additional bedding orientations were difficult to obtain due to the Ponce Limestone bedding around the fault segment being highly weathered and damaged. Two areas of bent strata layers were identified between the fault segments and are dragged along the fault segments suggesting left-lateral movement along the fault. The slope map supports this claim by showing 26° to 32° of slope change outlining the left-lateral curvature of the bent strata layers. The continuation of the bent strata layers on the opposite side of either of the fault segments could not

be identified. The A – A' profile shows no vertical offset where either of the fault segments are located, suggesting strike-slip movement controls this area.

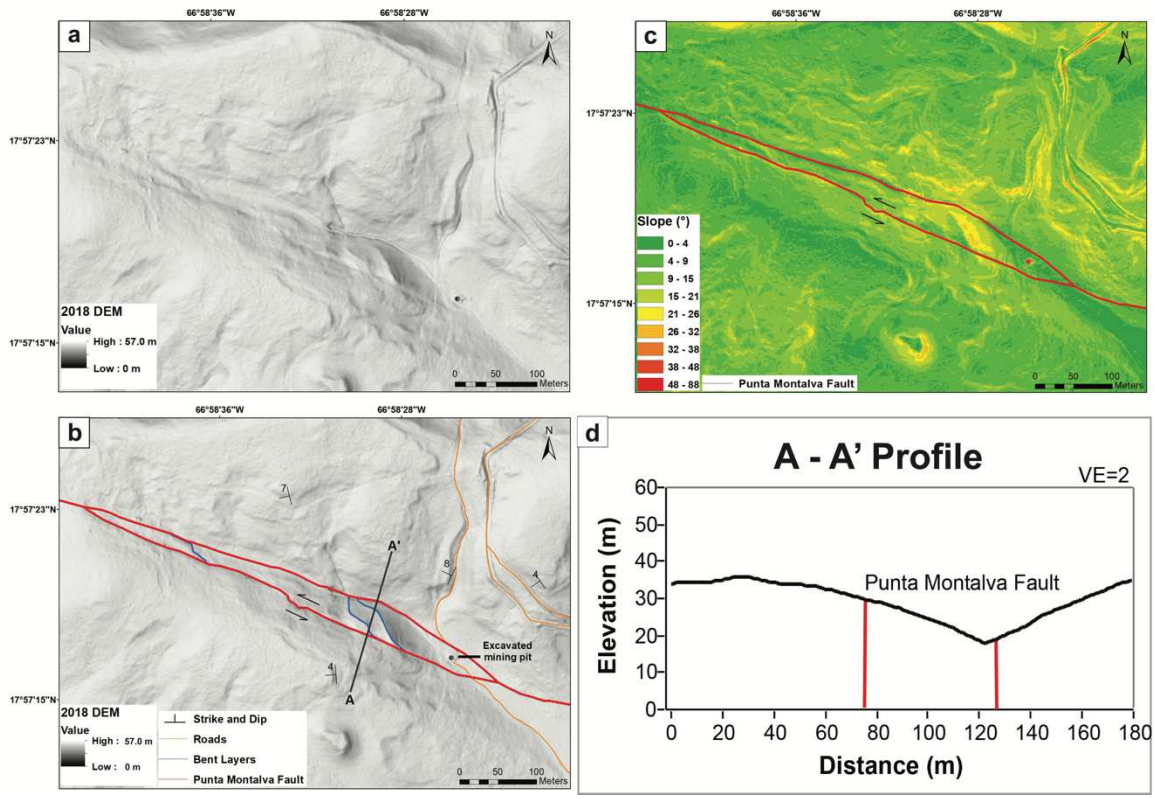


**Figure 7**: (a) Shaded relief map showing the topographic expression of the Punta Montalva Fault and bent strata layers using a multidirectional hillshade. (b) Shaded relief map showing the movement of the bent strata layers being controlled by the left-lateral strike-slip movement of the Punta Montalva Fault and the location of the A-A' profile. (c) Slope map depicting the degree of slope change defining the left-lateral curvature of the bent strata layers. (d) Profile depicting elevation against distance perpendicular to fault strike.

Fault segment 2, the largest of the exposed fault segments, is approximately 1,488 m long (Fig. 8). The width of this fault scarp is around 20 m wide on the northwestern and southeastern ends, but too thin to measure in the center. This fault segment left-laterally offsets an intermittent stream of approximately 132.6 m while also creating a drag fold along the fault segment. The orientation of bedding differs on the north and south sides of this fault segment with similar strikes and opposite dips to the north, and similar strikes and similar dips to the south. The bedding orientation north of the fault segment, west of the offset stream is 124°, 10°SW, and east of the offset stream 282°, 11°NE. The bedding orientation south of the fault segment, west of the offset stream is 241°, 8°NW, and east of the offset stream is 214°, 11°NW. The uppermost

section of the Ponce Limestone surrounding most of the fault segment contains substantial karst topography suggesting dissolution is occurring in the limestone. No evidence of karst topography was found in the lower sections of the Ponce Limestone. The B – B' profile shows vertical offset where fault segment 2 is located, suggesting strike-slip and normal fault movement have taken place.

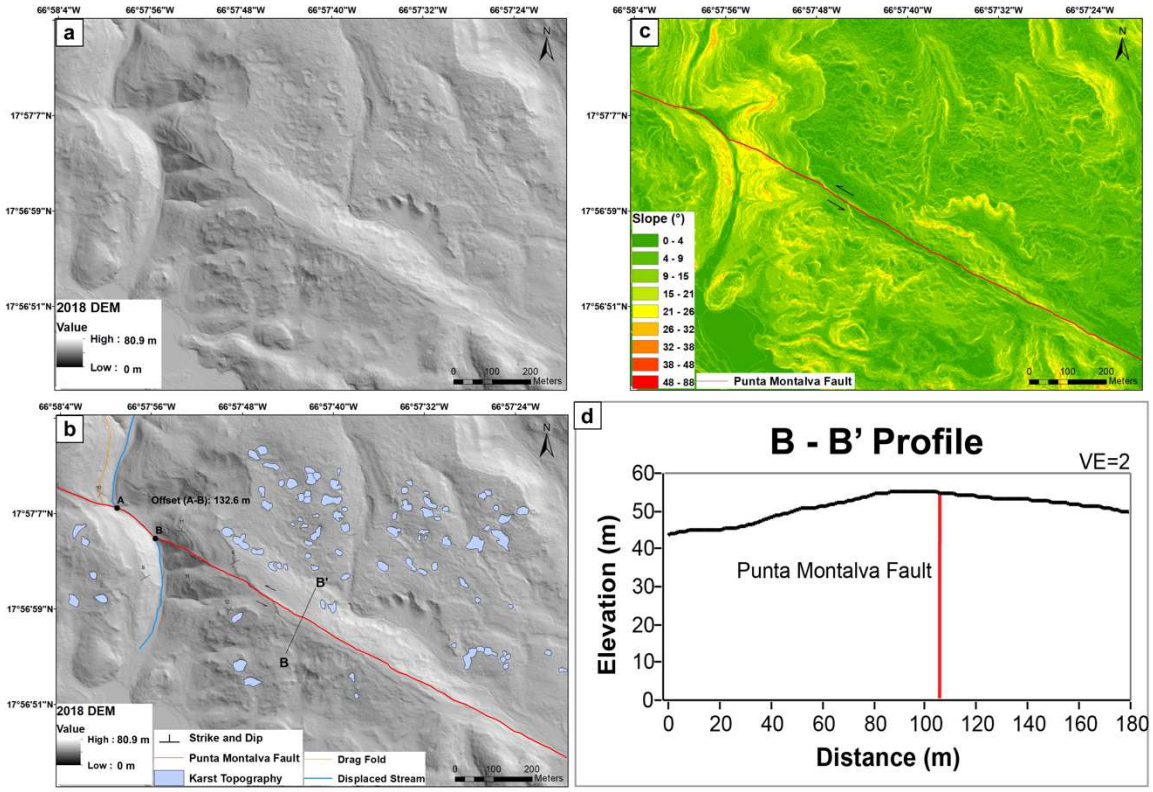


**Figure 8**: (a) Shaded relief map showing the topographic expression of the Punta Montalva Fault and the offset intermittent stream using a hillshade angle of 45°. (b) Shaded relief map showing the karst topography, drag fold, and the location of the B-B' profile. (c) Slope map depicting the degree of slope change. (d) Profile depicting elevation against distance perpendicular to fault strike.

Fault segment 3, the shortest of the exposed fault segments, is approximately 527 m long and the fault scarp is around 15 m wide (Fig. 9). The orientation of bedding differentiates from the north and south sides of the fault segment. Bedding orientation north of the fault segment is 325°, 6°NE, while bedding orientation south of the fault segment has similar strikes but opposing dips of 222°, 24°NW and 041°, 12°SE. This fault segment is embedded in Ponce Limestone but is mostly surrounded by alluvial deposits. The Ponce Limestone southwest of the fault segment has a steep slope ranging from 21° to 48°, while the Ponce Limestone northeast of the fault segment has a relatively shallow slope ranging from 0° to 21°. The C – C' profile shows a slight vertical

offset where this fault segment is located, suggesting a strike-slip component predominately controls this area with possibly the occurrence of minor normal fault movement.

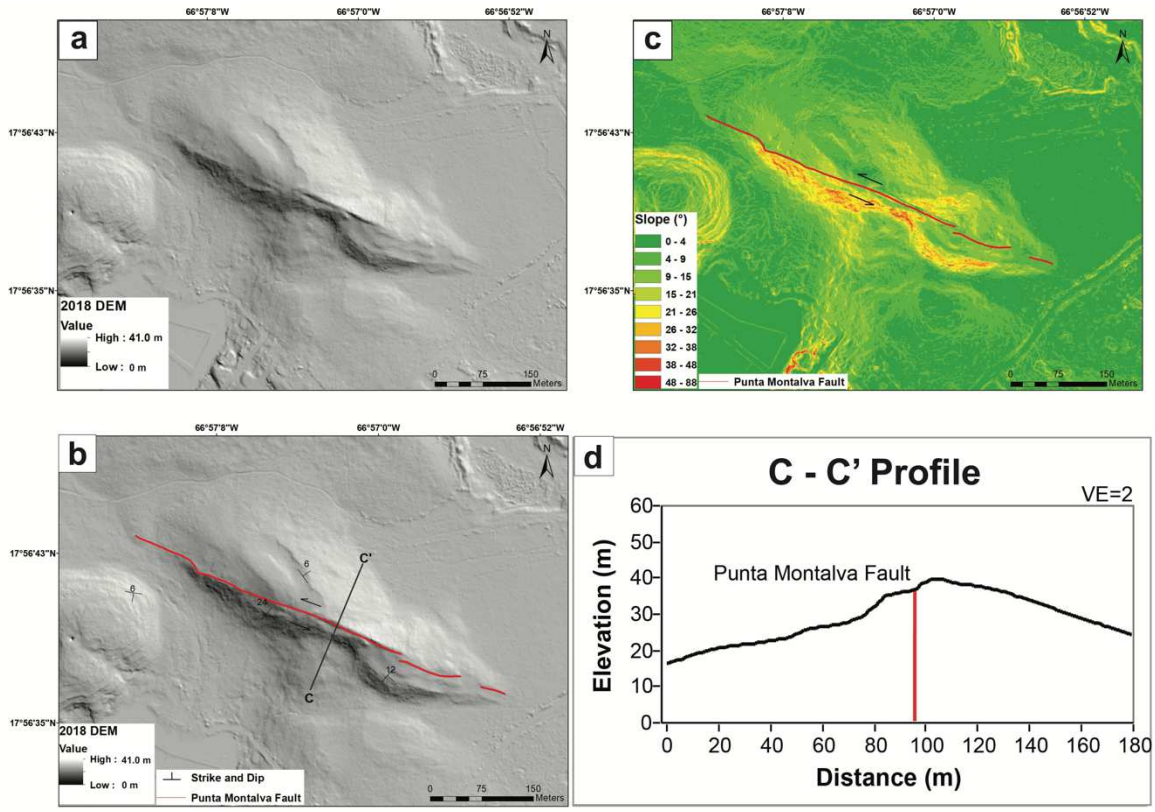


**Figure 9**: (a) Shaded relief map showing the topographic expression of the Punta Montalva Fault on the surface using a hillshade angle of 45°. (b) Shaded relief map showing the Punta Montalva Fault's trend from this study and the location of the C-C' profile. (c) Slope map depicting the degree of slope change along the Punta Montalva Fault. (d) Profile depicting elevation against distance perpendicular to the fault strike.

Northwest of fault segment 1 in Punta Montalva, a fault scarp was identified projecting off the coast that aligns with the trend of the Punta Montalva Fault (Fig. 10). The fault scarp strikes NW-SE and makes a high angle with the coastline. The slope map shows around 32° to 38° of slope change south of the fault scarp that contrasts with the areas to the north of it. Apart from the identified fault scarp, there was no distinguishable evidence of other faulting processes in the surrounding topography or bathymetry.

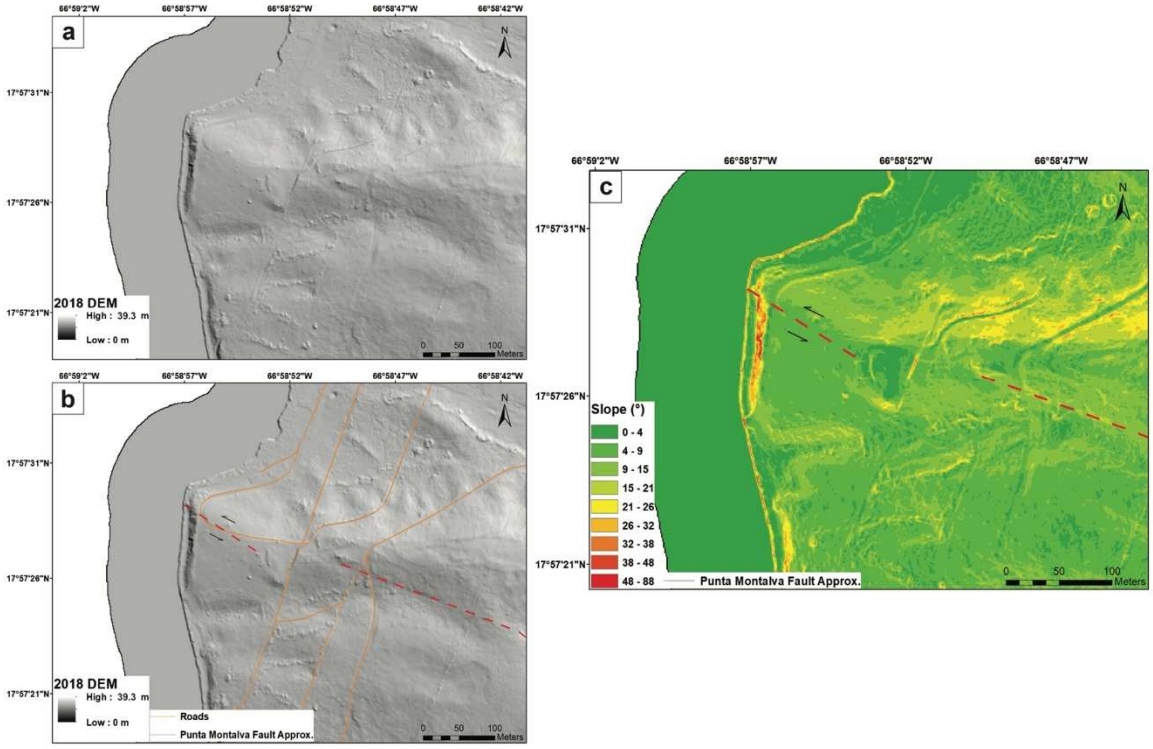


**Figure 10**: (a) Shaded relief map showing the topographic expression of the fault scarp on the coastline using a hillshade angle of 45°. (b) Shaded relief map showing the fault scarp in trend with the approximate location of the Punta Montalva Fault from this study. (c) Slope map depicting the degree of slope change along the fault scarp.

Offshore of the peninsula at Ensenada Las Pardas, two fault scarps were identified on what looks to be a marine shelf in the 2018 bathymetry DEM (Fig. 11). Both fault scarps have an E-W strike that aligns with the trend of the Punta Montalva Fault from this study and is collectively approximately 279 m long. The fault scarps do not display left-lateral movement but rather a vertical offset, suggesting that this part of the Punta Montalva Fault is dominated by normal faulting. There is no evidence of the fault scarp continuing further west. Three profile were constructed along the fault scarps perpendicular to their strike and all three profile indicate a fault is present. If the surface in the hanging wall matches the surface in the footwall, the approximate throw of the fault would be 1.4 m in Profile D, 2.4 m in Profile E, and 4.8 m in Profile F. Subsequent profile were constructed along the marine shelf surrounding the fault scarps to confirm the faults topographic expression in the profile were exclusive.

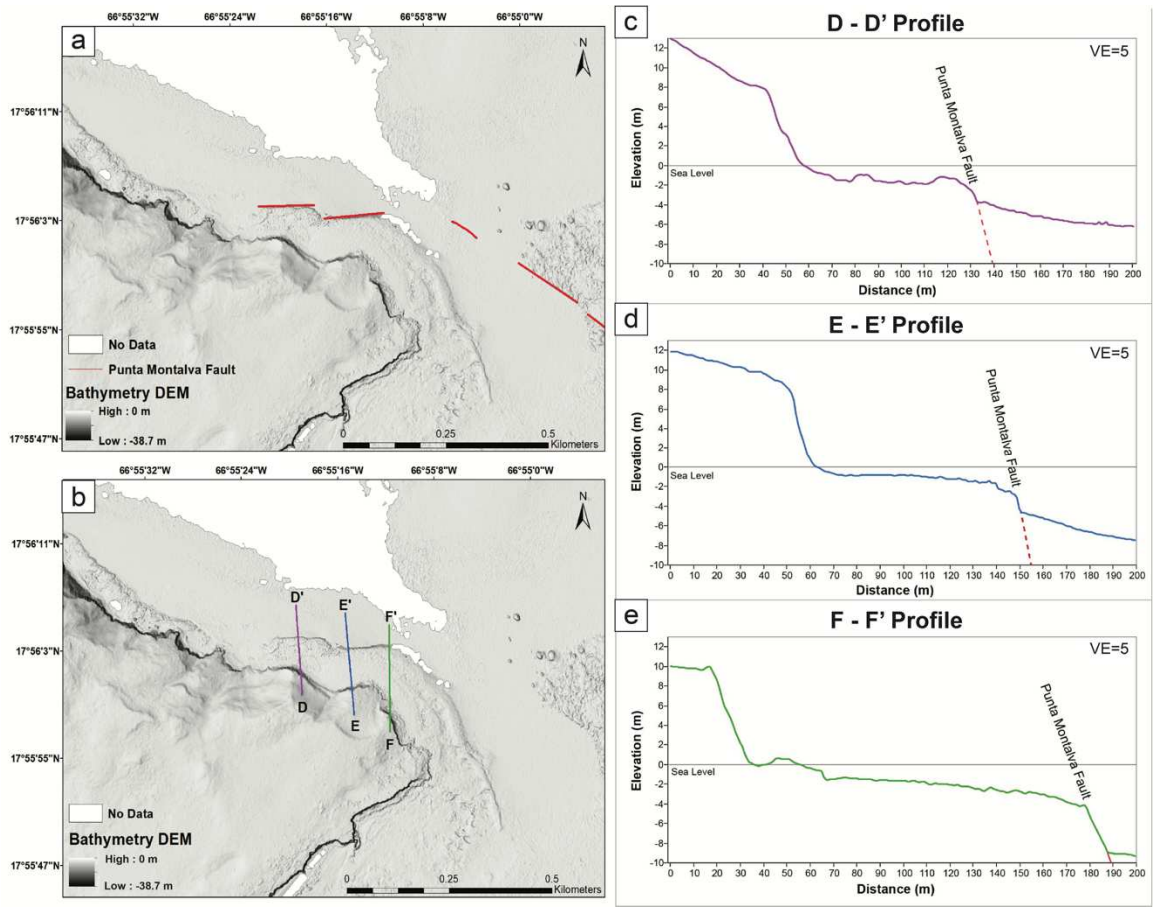


**Figure 11**: (a) Shaded relief map showing the fault scarps in the bathymetry using a multidirectional hillshade. (b) Shaded relief map showing the locations of the profile constructed perpendicular to the fault strike. (c, d, and e) Profiles depicting elevation against distance.

Further offshore of the peninsula at Ensenada Las Pardas, an additional fault scarp was identified in the 2018 bathymetry DEM (Fig. 12). The fault scarp is striking NW-SE that aligns with the trend of the Punta Montalva Fault from this study and is approximately 477 m long. The fault scarp displays left-lateral movement that has displaced seafloor topography approximately 98.3 m. Two profile graphs were constructed perpendicular to the fault's strike and indicate that a fault is present. The profile graphs show where the seafloor topography was once connected at around 9 m in depth where the fault scarp cuts through it, suggesting strike-slip movement controls this area.

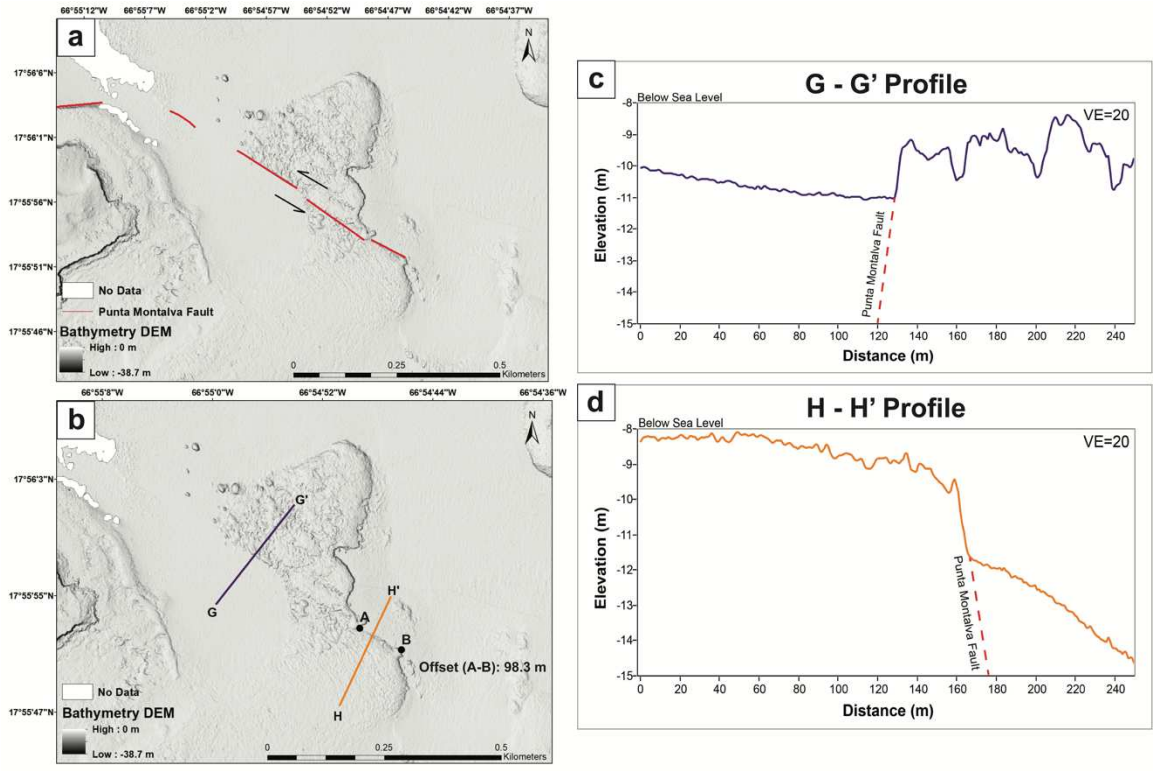


**Figure 12**: (a) Shaded relief map showing the fault scarp in the bathymetry using a multidirectional hillshade. (b) Shaded relief map showing the profiles constructed perpendicular to the fault strike. (c and d) Profiles depicting elevation against distance.

### *4.1.2 Vertical Differencing*

The vertical differencing results do not exhibit any noticeable systematic trends of vertical displacement along the Punta Montalva Fault that has occurred in the 14 years between 2004 and 2018 (Fig. 12). What the results do show is that at the very least the surrounding topography has changed. To visualize the results more prominently, the vertical differencing scale was set to a minimum of -2 m and a maximum of 2 m. The positive (blue) and negative (red) vertical differencing values displayed in the DEM topographic hillshade represent upward and downward changes in topography. Yellow indicates that little to no vertical displacement has occurred. In the northwest near Punta Montalva, the vertical differencing results show localized areas of downward changes in topography. In the southeast on the peninsula near Ensenada Las Pardas, there were relatively no changes in topography aside from on the coastline. The cliffsides along the coast off the peninsula show downward changes in topography. However, there is one area of the cliffside that strongly displays 2 m of upward displacement.

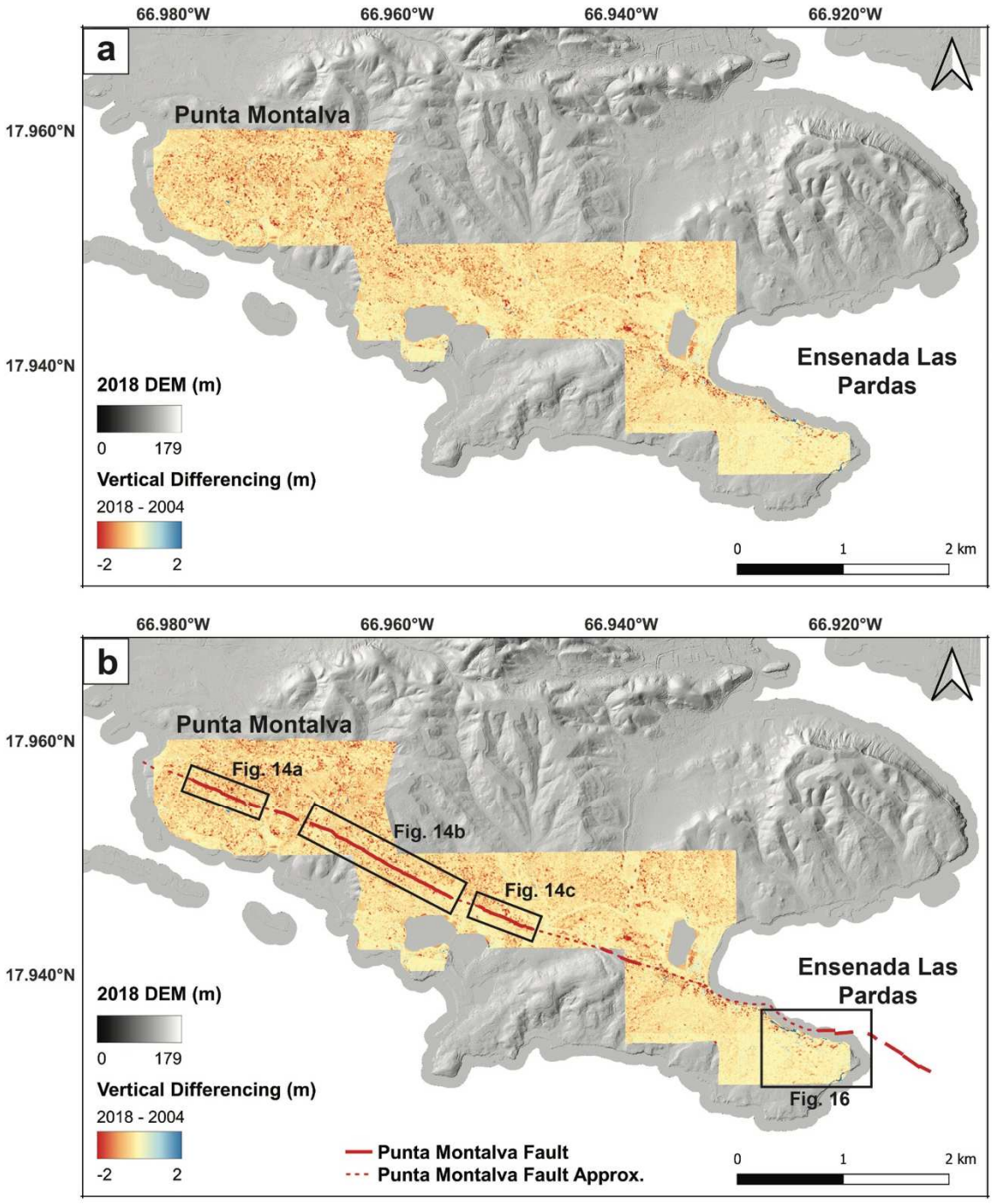


**Figure 13**: DEM topographic hillshade of the 2018-2004 vertical differencing results depicting upward and downward changes in topography layered on top of a shaded relief map using a hillshade angle of 315°. The red line is the Punta Montalva Fault's trend from this study.

The vertical differencing results along fault segment 1 and fault segment 2 do not show any vertical offset. The results do show small areas, mostly downward changes in topography, around the fault segments that suggest either subsidence or erosion has occurred. The vertical differencing results along fault segment 3 show around 2 m of upward change in topography along a small area north of the fault segment.

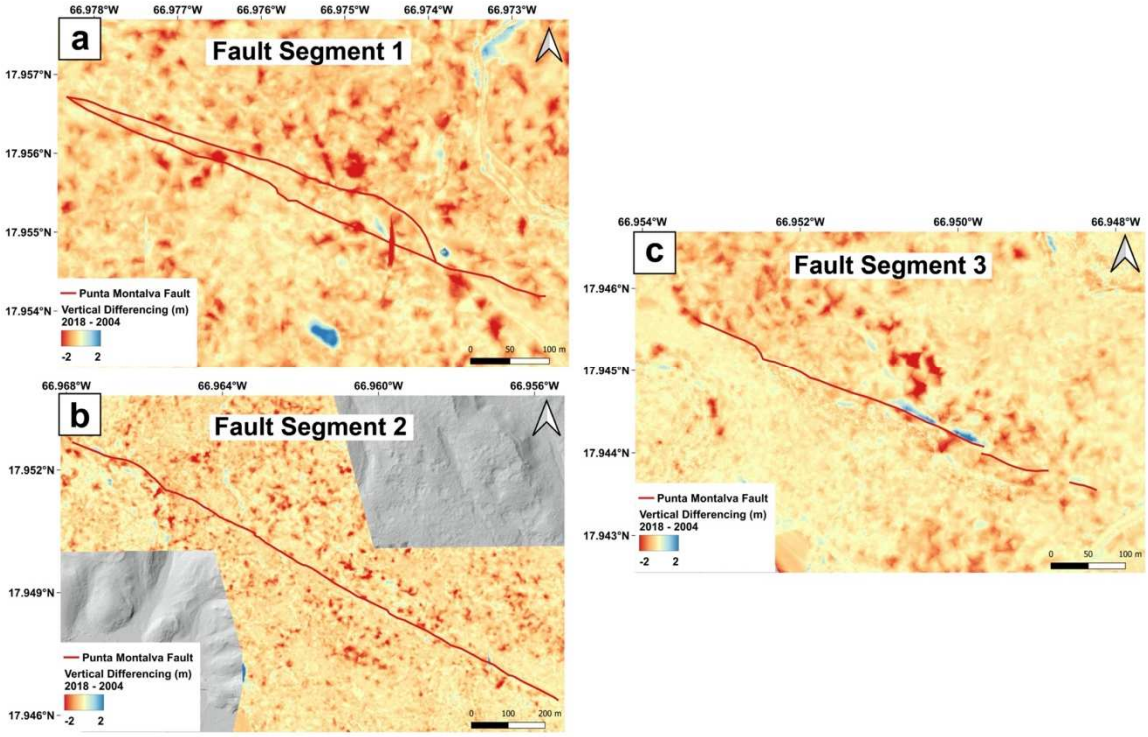


**Figure 14**: DEM topographic hillshades of the 2018-2004 vertical differencing results depicting upward and downward changes in topography along fault segments 1, 2, and 3.

*4.2 Discussion*

*4.2.1 Fault Structure and Segmentation*

High-resolution mapping portion of this study has provided an updated delineation of the Punta Montalva Fault that more accurately characterizes its spatial extent on the surface and at shallow bathymetry. Moreover, it defines a new segmentation and structure discussed below.

Fault segment 1 was the only fault segment identified that was comprised of two parallel faults. The bedding orientations of the Ponce Limestone around this fault segment are sub-horizontal and shallowly dipping. The S-shaped geometry of layers suggest that a second fault has to be present to be able to deform the Ponce Limestone in such a way. The new fault was

traced from where it connects to the main fault segment in the northwest to where it connects to the main fault segment in the southeast. Following the duplex model proposed by Woodcock and Fischer (1986), the bent strata layers are being interpreted as duplex structures that are being controlled left-laterally by the two fault segments. The A – A' profile (Fig. 7d) shows no vertical displacement along either of the fault segments, leading to the interpretation that this fault segment is dominated by strike-slip movement.

Fault segment 2 exhibits the most amount of horizontal offset out of all the fault segments. The offset intermittent stream was measured to be horizontally displaced by fault segment 2 at approximately 132.6 m, which contrasts with Addarich-Martínez's (2009) initial offset measurement of approximately 200 m. Two bedding orientations south of the fault segment on either side of the intermittent stream are on average striking NE with a shallow dip (Fig. 8c). Two bedding orientations north of the fault segment on either side of the intermittent stream are both striking NW but are shallowly dipping in opposite directions (Fig. 8c). The many sink holes found around fault segment 2 contrasts with Addarich-Martínez's (2009) interpretation of the karst topography not being common in the Ponce Limestone formation. Due to the thick vegetation and difficulty to access, the karst topography would have been challenging to identify in the field. Karst topography was not found in the Ponce Limestone around fault segment 1 or fault segment 3, suggesting differing lithology of the uppermost layer of the Ponce Limestone around fault segment 2. The B – B' profile (Fig. 8d) shows a small amount of downwards vertical offset where fault segment 2 is located, suggesting the occurrence of normal fault movement.

Fault segment 3 exhibits the most prominent surface exposure compared to fault segments 1 and 2. The continuation of the fault segment northwest towards fault segment 2 could not be identified due to the overlying alluvium deposits. There was no evidence in the data or any signs of deformation that suggest that the shutter ridge proposed by Adames-Corraliza (2017) is present. Rather the structure demonstrates sub-horizontal layered bedding with an orientation of 099°, 6°SW. The C – C' profile (Fig. 9d) shows a small amount of downwards vertical offset where fault segment 3 is located, suggesting the occurrence of normal fault movement.

The fault scarp identified in the northwest of fault segment 1 in Punta Montalva (Fig. 10) gave a new rendition of where the Punta Montalva Fault projects off the coast. The original interpretation by Addarich-Martínez (2009) showed the Punta Montalva Fault projecting off the coast further north (Fig. 15). It is also thought that the Punta Montalva Fault is part of the NBPMFZ, a through-going left-lateral strike-slip fault zone that cuts through the Lajas Valley

(Fig. 3; Roig-Silva et al., 2013). There was no evidence found in the bathymetry that suggests the Punta Montalva Fault projects further northwest into La Parguera, suggesting that the proposed NBPMFZ is not continuous.

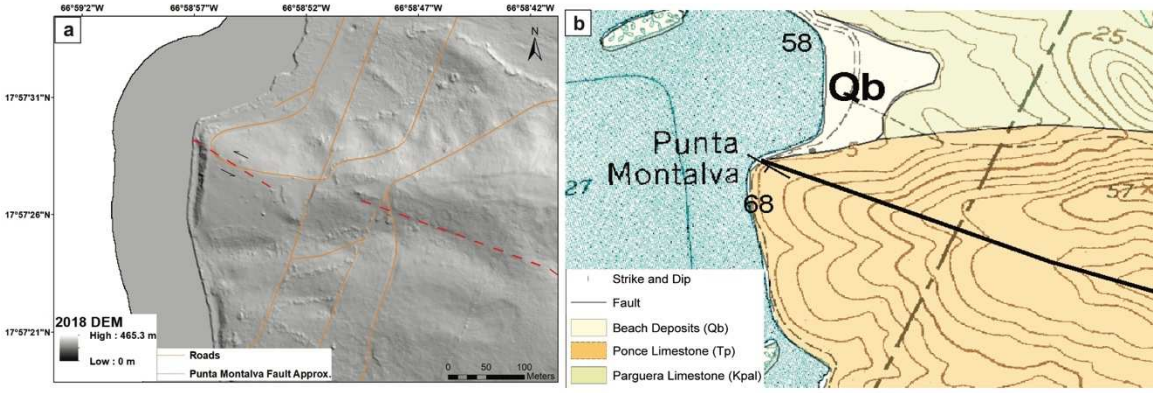


**Figure 15**: (a) Shaded relief map showing the fault scarp in trend with the approximate location of the Punta Montalva Fault from this study using a hillshade angle of 45°. Arrows indicate left-lateral movement. (b) Addarich-Martínez's (2009) interpretation of the projection of the Punta Montalva Fault in his geologic map of the Guánica Quadrangle.

The fault scarps found in the bathymetry off the coast of the peninsula at Ensenada Las Pardas are interpreted to be the southeastern seaward extension of the Punta Montalva Fault. The first bathymetry fault scarp that strikes E-W (Fig. 11) along a marine shelf was the only fault identified that exclusively portrays normal fault movement. The second bathymetry fault scarp that strikes NW-SE (Fig. 12), approximately 349 m southeast of the first fault scarp, displays left-lateral strike-slip movement. The G – G' and H – H' profile graphs (Fig. 12c and 12d) show where the fault scarp horizontally offsets seafloor topography. At first glance, the fault lines in the profile graphs look to be formed by normal fault movement, but it is showing the maximum and minimum depths where this seafloor topography was once connected. The discovery of these bathymetry fault scarps leads to the assumption that the Punta Montalva Fault extends further offshore than originally thought. Using high-resolution seismic reflection profiles, ten Brink et al. (2022) identified multiple sub-vertical faults on the insular shelf offshore of the peninsula at Ensenada Las Pardas that are parallel with the bathymetry fault scarps, furthering the suggestion that the Punta Montalva Fault extends southeast offshore.

### *4.2.2 Vertical Differencing*

The subtraction of the 2004 DTM from the 2018 DTM concluded that there has not been significant vertical displacement along the Punta Montalva Fault in the 14 years. Although

vertical displacement could not be determined along the Punta Montalva Fault, the results provided insight regarding the lack of recent slip the fault has undergone between 2004 to 2018.

Generally, the vertical differencing results show mostly downward changes in topography, specifically in the northwest near Punta Montalva. The localized downward changes in topography near Punta Montalva could be a result of subsidence or erosion, or possibly be related to some form of karst subsidence also seen around fault segment 2 (Fig. 8).

In the southeast on the coast of the peninsula at Ensenada Las Pardas, the cliffsides also show downward changes in topography, which was expected. This occurrence is most likely a result of structural erosion from various sea activity. What was not expected was the 2 m of upward change in topography along a ~600 m long section of the cliffside. It seemed unlikely that this occurred from natural causes and was more reasonable to suspect an error related to the construction of the 2004 DTM. The technology used to acquire the 2004 LiDAR dataset was older and has larger errors compared to the 2018 LiDAR dataset. Las2dem, the software used to create the 2004 and 2018 DTMs, uses the Triangulated Irregular Network (TIN) interpolation method to build DEMs from LiDAR point clouds. This could have been an issue considering the 2004 LiDAR dataset has 1,139,736 ground classified points while the 2018 LiDAR dataset has 134,160,181 ground classified points. The TIN interpolation method creates a surface formed from triangles of nearest neighbor points. The more points you have, the smoother and more accurate the surface will be. The fewer points you have, the more jagged and less accurate the surface will be. The 2004 LiDAR dataset had a significantly lower number of points taken along the coastline compared to the 2018 LiDAR dataset. When the 2004 DTM was created, the software may have interpolated this specific area of the coastline at a lower elevation than it actually is since there were not enough data points to draw from (Fig. 16). It is exceedingly probable that the misinterpolation produced the 2 m of upward change in topography in the vertical differencing results. Considering this, there is also a possibility that the misinterpolation caused by the lack of data points in the 2004 LiDAR dataset could have affected other areas in the vertical differencing results as well. This possibility led to the decision not to trust any of the vertical differencing results. To accurately perform vertical differencing in the future, it would be recommended to use two datasets with a similar number of ground classified points.

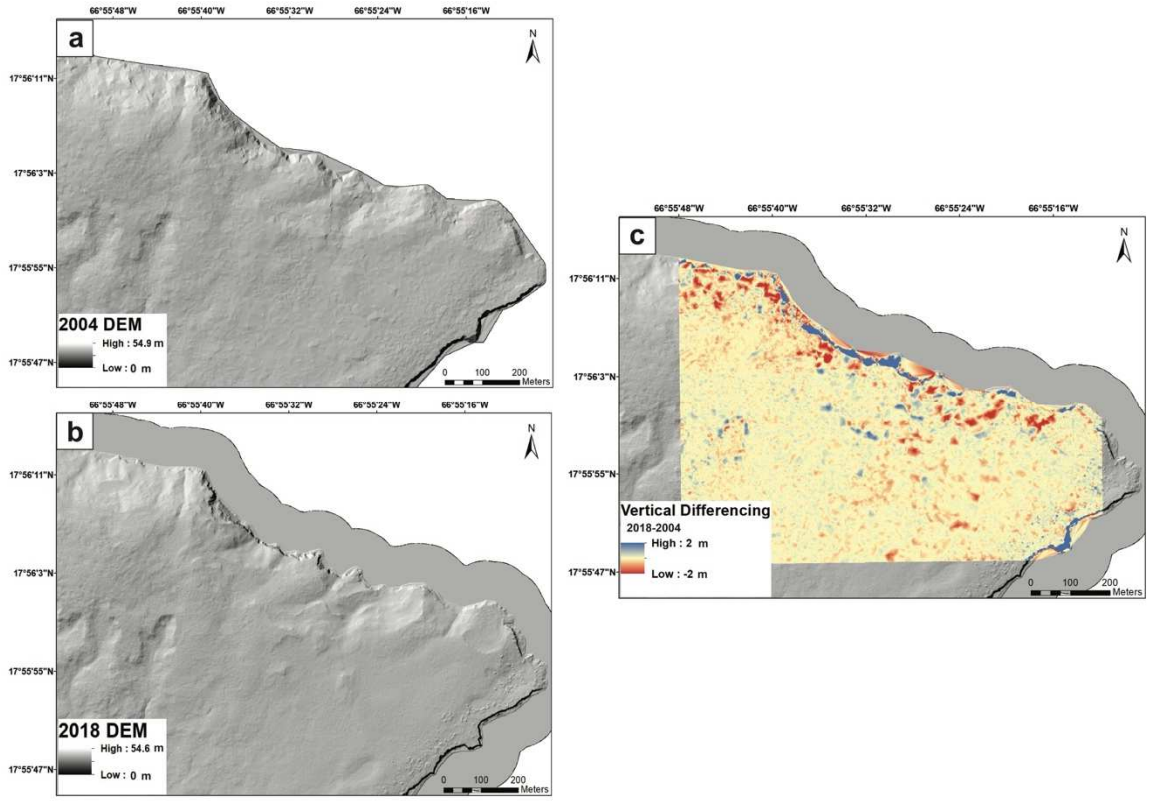


**Figure 16**: (a) Shaded relief map of the 2004 LiDAR dataset using a hillshade angle of 315° showing the jagged appearance of the coastline due to a lack of data points. (b) Shaded relief map of the 2018 LiDAR dataset using a hillshade angle of 315° showing a more detailed interpolation of the coastline due to a sufficient amount of data points. (c) DEM topographic hillshade of the vertical differencing results depicting the 2 m of upward change in topography along the coastline.

### *4.2.3 Implications for Seismic Hazards*

Our observations suggest that the Punta Montalva Fault is segmented on the surface and at shallow bathymetry, not continuous. The Punta Montalva Fault being segmented correlates to the recent seismic activity that is being accommodated by many small faults instead of large mature ones (ten Brink et al., 2022). One hypothesis suggested by ten Brink et al. (2022) as to why many small faults in the area have not formed into one large fault yet is due to the low deformation rate. The deformation rate in the NE Caribbean is approximately 1-2 mm/yr, consequently making the formation of many small faults into one large fault take more time (ten Brink et al., 2022). If the Punta Montalva Fault is segmented like our observations suggest, then it would have a lower seismic hazard. However, the seismic hazard would increase if the segmented Punta Montalva Fault one day forms into a large continuous fault.

### *4.2.4 Strain Accommodation*

The Punta Montalva Fault displayed both left-lateral strike-slip and normal fault movement in our observations, leading to the implication of transtension. This would make the dominantly strike-slip fault have a NW-SE component of extensional deformation. The extensional component in our observations coincide with the tectonic deformation model proposed by ten Brink et al. (2022) of the extension due to locking in the Muertos Trough and sinking in the Puerto Rico Trench. Fusion of the southern edge of the Puerto Rico block with the Muertos Trough, while the rest of the block is dragged north into the Puerto Rico Trench, would cause the NW-SE extensional component along the Punta Montalva Fault. Furthermore, implication of transtension along the Punta Montalva Fault coincides with the second tectonic deformation model proposed by ten Brink et al. (2022) of the Western Puerto Rico Deformation Boundary. This deformation boundary is suggested to be driven by various seismic coupling on the subduction interface of Puerto Rico with high coupling in the Mona Passage, which contains NW-SE striking faults that possibly extend eastward on land into southwestern Puerto Rico (ten Brink et al., 2022). The seismic activity reported by ten Brink et al. (2022) suggested NW-SE extension offshore of southwestern Puerto Rico where the Punta Montalva Fault is located, furthering the NW-SE transtentional strain accommodation we are seeing in our observations. The Western Puerto Rico Deformation Boundary is a more appropriate model for the strain accommodation occurring in the area since the model includes both a left-lateral strike-slip and an extensional component, instead of just an extension component that was proposed in the extension due to locking in the Muertos Trough and sinking in the Puerto Rico Trench model.

# CHAPTER V

## CONCLUSIONS

High-resolution mapping and vertical differencing over the Punta Montalva Fault were completed using multiple DEMs derived from airborne LiDAR surveys. The Punta Montalva Fault is comprised of three exposed fault segments on the surface and two fault scarps in the bathymetry that are moderately distributed and trending approximately 110° to 115° from Punta Montalva to Ensenada Las Pardas. The total length of the Punta Montalva Fault if continuous underneath the surface is 7.97 km. Both strike-slip and normal faulting movement was detected along the fault resulting in a transtensional deformation zone. The DEM revealed scarps, dragged layers, and a duplex structure that support the NW-SE left-lateral movement of the fault. There was no evidence found that suggested the Punta Montalva Fault extends further northwest into La Parguera. Fault scarps identified in the bathymetry off the peninsula at Ensenada Las Pardas are interpreted to be the southeastern seaward extension of the Punta Montalva Fault and present the possibility that the fault extends even further offshore to the southeast. Vertical differencing results along the Punta Montalva Fault were unconclusive due to poor quality of the 2004 DEM.

# REFERENCES


Adames-Corraliza, Á. R. (2017). *Geomorphic and geophysical characterization of the north Boquerón Bay-Punta Montalva fault zone: A capable fault system in southwestern Puerto Rico* (Doctoral dissertation).

Addarich-Martínez, L. (2009). *The geologic mapping and history of the Guánica Quadrangle, southwestern Puerto Rico* (Doctoral dissertation).

Albino, F., Smets, B., d'Oreye, N., & Kervyn, F. (2015). High□resolution TanDEM□X DEM: An accurate method to estimate lava flow volumes at Nyamulagira Volcano (DR Congo). *Journal of Geophysical Research: Solid Earth*, *120*(6), 4189-4207.

Benford, B., DeMets, C., & Calais, E. (2012). GPS estimates of microplate motions, northern Caribbean: evidence for a Hispaniola microplate and implications for earthquake hazard. *Geophysical Journal International*, *191*(2), 481-490.

Calais, E., Mazabraud, Y., Mercier de Lépinay, B., Mann, P., Mattioli, G., & Jansma, P. (2002). Strain partitioning and fault slip rates in the northeastern Caribbean from GPS measurements. *Geophysical Research Letters*, *29*(18), 3-1.

Chaytor, J. D., & Uri, S. (2010). Extension in mona passage, Northeast Caribbean. *Tectonophysics*, *493*(1-2), 74-92.

Clark, K. J., Nissen, E. K., Howarth, J. D., Hamling, I. J., Mountjoy, J. J., Ries, W. F., ... & Strong, D. T. (2017). Highly variable coastal deformation in the 2016 Mw7. 8 Kaikōura earthquake reflects rupture complexity along a transpressional plate boundary. *Earth and Planetary Science Letters*, *474*, 334-344.

Dolan, J. F., Mullins, H. T., Wald, D. J., & Mann, P. (1998). Active tectonics of the north-central Caribbean: Oblique collision, strain partitioning, and opposing subducted slabs. *Special Papers-Geological Society of America*, 1-62.

Flores, C. H., Ten Brink, U., & Bakun, W. H. (2012). Accounts of damage from historical earthquakes in the northeastern Caribbean, to aid in the determination of their location and intensity magnitudes. *US Department of the Interior, US Geological Survey*.

Huérfano, V., von Hillebrandt-Andrade, C., & Báez-Sanchez, G. (2005). Microseismic activity reveals two stress regimes in southwestern Puerto Rico. *Active tectonics and seismic hazards of Puerto Rico, the Virgin Islands, and offshore areas*, *385*, 81-101.

Izumida, A., Uchiyama, S., & Sugai, T. (2017). Application of UAV-SfM photogrammetry and aerial lidar to a disastrous flood: repeated topographic measurement of a newly formed crevasse splay of the Kinu River, central Japan. *Natural Hazards and Earth System Sciences*, *17*(9), 1505-1519.

Jansma, P. E., Mattioli, G. S., & Mann, P. (2005). GPS results from Puerto Rico and the Virgin Islands: Constraints on tectonic setting and rates of active faulting. *Active Tectonics and Seismic Hazards of Puerto Rico, the Virgin Islands, and Offshore Areas*, *385*, 13-30.

Jansma, P. E., Mattioli, G. S., Lopez, A., DeMets, C., Dixon, T. H., Mann, P., & Calais, E. (2000). Neotectonics of Puerto Rico and the Virgin Islands, northeastern Caribbean, from GPS geodesy. *Tectonics*, *19*(6), 1021-1037.

Joyce, J., McCann, W. R., & Lithgow, C. (1987). Onland active faulting in the Puerto Rico platelet. *Eos (Transactions, American Geophysical Union)*, *68*, 1483.

Kaye, C. A. (1957). Notes on the structural geology of Puerto Rico. *Geological Society of America Bulletin*, *68*(1), 103-118.

Llerandi-Roman, P. A. (2004). The Geology of the western section of the Sabana Grande quadrangle: implications for the geological evolution of southwestern Puerto Rico. University of Puerto Rico, Mayaguez (Puerto Rico).

Krushensky, R. D., & Monroe, W. H. (1979). Geologic map of the Yauco and Punta Verraco quadrangles, Puerto Rico (No. 1147).

López, A.M., Hughes, K.S., & Vanacore, E. (2020), Puerto Rico's Winter 2019-2020 Seismic Sequence Leaves the Island On Edge, Temblor, http://doi.org/10.32858/temblor.064.

Lucieer, A., Jong, S. M. D., & Turner, D. (2014). Mapping landslide displacements using Structure from Motion (SfM) and image correlation of multi-temporal UAV photography. *Progress in Physical Geography*, *38*(1), 97-116.

Mann, P., Hippolyte, J. C., Grindlay, N. R., & Abrams, L. J. (2005). Neotectonics of southern Puerto Rico and its offshore margin. *Active tectonics and seismic hazards of Puerto Rico, the Virgin Islands, and offshore areas*, *385*, 173-214.

Martinez-Torres, L. M., Lopetegui, A., & Eguiluz, L. (2012). Automatic resolution of the three-points geological problem. *Computers & Geosciences*, *42*, 200-202.

Masson, D. G., & Scanlon, K. M. (1991). The neotectonic setting of Puerto Rico. *Geological Society of America Bulletin*, *103*(1), 144-154.

McCann, W. R., & Pennington, W. D. (1990). Seismicity, large earthquakes, and the margin of the Caribbean plate, The Caribbean region, The Geology of North America. *H G. Dengo, J. Case*, 291-306.

Monroe, W. H. (1980). Geology of the middle Tertiary formations of Puerto Rico (No. 953). US Government Printing Office.

Ocasio, D. M. (2004). An offshore total□intensity magnetic study of Boquerón Bay area, southwest Puerto Rico. *Undergraduate Research Investigations, Department of Geology, University of Puerto Rico, Mayagüez*.

Oskin, M. E., Arrowsmith, J. R., Corona, A. H., Elliott, A. J., Fletcher, J. M., Fielding, E. J., ... & Teran, O. J. (2012). Near-field deformation from the El Mayor–Cucapah earthquake revealed by differential LIDAR. *Science*, *335*(6069), 702-705.

Prentice, C. S., & Mann, P. (2005). Paleoseismic study of the South Lajas fault: First documentation of an onshore Holocene fault in Puerto Rico (Vol. 385, pp. 215-222). Geological Society of America Special Paper.

Rivera-Santiago, F. (2009). Geomorphic and geologic features of the Punta Montalva Fault, *Undergraduate Research Investigations*, Department of Geology, University of Puerto Rico, Mayagüez.

Roig-Silva, C. (2003). The origins of topographic lineaments of the Punta Montalva area, *Undergraduate Research Investigations*, Department of Geology, University of Puerto Rico, Mayagüez.

Roig□Silva, C., Asencio, E., & Joyce, J. (2009). The North Boquerón Bay–Punta Montalva Fault zone; a thorough going active fault system in southwestern Puerto Rico. In *Geological Society of America Annual Meeting, Portland, Oregon, Paper* (No. 173-3).

Roig, C., & Asencio, E. (2007). Geophysics for Quaternary-fault mapping in Cabo Rojo, Puerto Rico. In *20th EEGS Symposium on the Application of Geophysics to Engineering and Environmental Problems* (pp. cp-179). European Association of Geoscientists & Engineers.

Roig□Silva, C. M., Asencio, E., & Joyce, J. (2013). The northwest trending North Boquerón Bay□ Punta Montalva Fault zone; a thorough going active fault system in southwestern Puerto Rico. *Seismological Research Letters*, *84*(3), 538-550.

Scott, C. P., Arrowsmith, J. R., Nissen, E., Lajoie, L., Maruyama, T., & Chiba, T. (2018). The M7 2016 Kumamoto, Japan, earthquake: 3□D deformation along the fault and within the damage zone constrained from differential lidar topography. *Journal of Geophysical Research: Solid Earth*, *123*(7), 6138-6155.

Scott, C., Phan, M., Nandigam, V., Crosby, C., & Arrowsmith, R. (2021). Measuring change at Earth's surface: On-demand vertical and three-dimensional topographic implemented in OpenTopography: *Geosphere*, (Vol. 17). https://doi.org/10.1130/GES02259.1.

ten Brink, U. S., Vanacore, E. A., Fielding, E. J., Chaytor, J. D., López□Venegas, A. M., Baldwin, W. E., ... & Andrews, B. D. (2022). Mature diffuse tectonic block boundary revealed by the 2020 southwestern Puerto Rico seismic sequence. *Tectonics*, *41*(3), e2021TC006896.

US Census Bureau, 2021, Table 2. Resident Population for the 50 States, the District of Columbia, and Puerto Rico: 2020 Census, Retrieved from https://www.census.gov/data/tables/2020/dec/2020-apportionment-data.html.

Vičič, B., Momeni, S., Borghi, A., Lomax, A., & Aoudia, A. (2021). The 2019-2020 Indios, Puerto Rico earthquake sequence: seismicity and faulting. [In revision].

Volckmann, R. P. (1984). Geologic map of the Cabo Rojo and Parguera quadrangles, southwest Puerto Rico (No. 1557).

Woodcock, N. H., & Fischer, M. (1986). Strike-slip duplexes. *Journal of structural geology, 8*(7), 725-735.

VITA

Lauren Jane Weilert

Candidate for the Degree of

Master of Science

Thesis: FAULT STRUCTURE OF THE PUNTA MONTALVA FAULT USING HIGH-RESOLUTION DEMS

Major Field: Geology

Biographical:

Education:

Completed the requirements for the Master of Science in Geology at Oklahoma State University, Stillwater, Oklahoma in July, 2022.

Completed the requirements for the Bachelor of Science in Geology at Oklahoma State University, Stillwater, Oklahoma in 2020.

Experience: Analyzed the geometry, sense of displacement, and history of the formation over the Seneca Fault in Disney, Oklahoma using digital elevation models and well data. Conducted electrical resistivity in the Multiple-arch buttresses of the Pensacola Dam in Disney, Oklahoma. Constructed digital elevation models from photogrammetry derived from an Unmanned Aerial Vehicle in Structure from Motion software.

Professional Memberships: American Geophysical Union (AGU), Geological Society of America (GSA), and Association of Women Geoscientists (AWG).